3D VISUALIZATION AND MAPPING OF CHOROID THICKNESS BASED ON OPTICAL COHERENCE TOMOGRAPHY: A STEP-BY-STEP GEOMETRIC APPROACH

V. Kiran Kumar[1] *T. Ritesh Chandra*[2] *Soumya Jana*[1] *A. Richhariya*[3] *J. Chhablani*[3]

[1]Department of Electrical Engineering, IIT Hyderabad, Andhra Pradesh, India-502205
[2]School of Electrical Sciences, IIT Bhubaneswar, Odisha, India-751005
[3]L. V. Prasad Eye Institute, Hyderabad, Andhra Pradesh, India-500034

ABSTRACT

Although bodily organs are inherently 3D, medical diagnosis often relies on their 2D representation. For instance, sectional images of the eye (especially, of its posterior part) based on optical coherence tomography (OCT) provide internal views, from which the ophthalmologist makes medical decisions about 3D eye structures. In the course, the physician is forced to mentally synthesize the underlying 3D context, which could be both time consuming and stressful. In this backdrop, can such 2D sections be arranged and presented in the natural 3D form for faster and stress-free diagnosis? In this paper, we consider ailments affecting choroid thickness, and address the aforementioned question at two levels — in terms of 3D visualization and 3D mapping. In particular, we exploit the spherical geometry of the eye, align OCT sections on a nominal sphere, and extract the choroid by peeling off inner and outer layers. At each step, we render our intermediate results on a 3D lightfield display, which provides a natural visual representation. Finally, the thickness variation of the extracted choroid is spatially mapped, and observed on a lightfield display as well as using 3D visualization softwares on a regular 2D terminal. Consequently, we identified choroid depletion around optic disc based on the test OCT images. We believe that the proposed technique would provide ophthalmologists with a tool for making faster diagnostic decisions with less stress.

Index Terms— Optical coherence tomography (OCT), Spherical alignment, Choroid thickness, 3D visualization, Lightfield display.

1. INTRODUCTION

Present advancements in the field of medical imaging facilitate doctors to understand and diagnose complex medical conditions. For instance, certain eye ailments, which deplete tiny blood vessels in the inner walls of the posterior part, have traditionally been difficult to detect. The complexity arises because the rear portion of the eye consists of various layers (refer Fig. 1 for a high level depiction of the sagittal crossection),

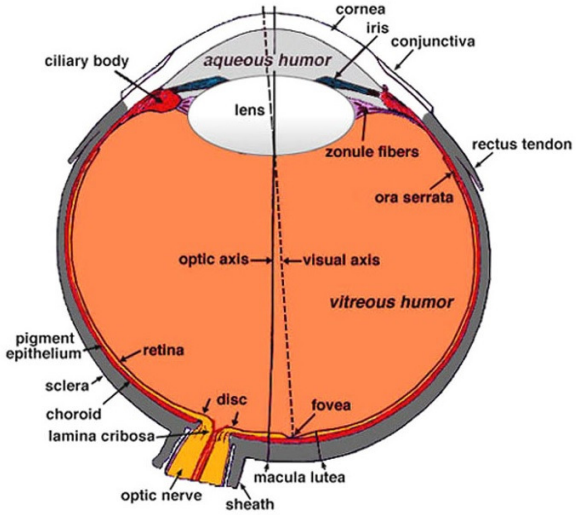

Fig. 1: Sagittal cross section of adult human eye [1]

and the blood vessels of interest lie sandwiched between retinal pigment epithelium (RPE) and sclera forming the choroid layer. Medical diagnosis of such diseases has considerably improved with the advent of *Optical Coherence Tomography (OCT)*, an advanced subsurface imaging technique. In this context, choroid thickness estimated from OCT images of the posterior part of the eye has emerged as an important determinant. Specifically, estimation accuracy (in terms of diagnostic outcome), and visual representation have assumed significance in studying choroid thickness distribution. In this paper, we provide a step-by-step geometric approach towards 3D mapping of choroid thickness, and its visualization on a 3D lightfield display.

Typical OCT images are shown in Fig. 2. In each image, the right part depicts an OCT slice, consisting of vitreous humor (black), retina, RPE (bright), choroid (granular) and sclera, from top to bottom. The left portion of the image, called *en-face*, depicts the face-on view of retina, the innermost layer, while the dotted line indicates the vertical location of the OCT plane. Usually, the ophthalmologist flips

978-1-4799-3203-0/13/$31.00

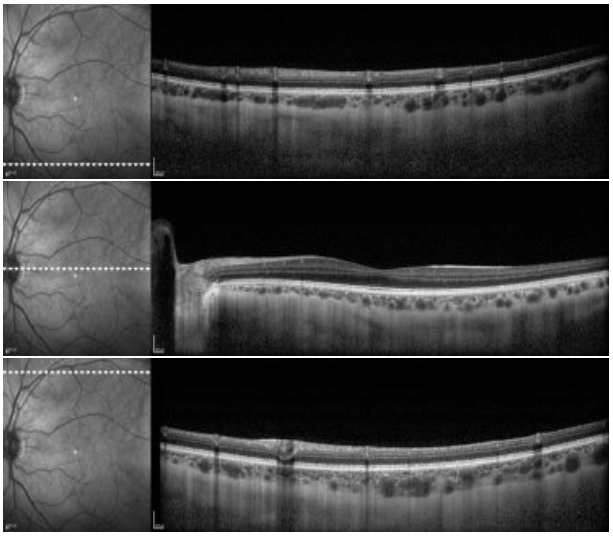

Fig. 2: The 1-st, 16-th and 31-st of the 31 OCT images of the posterior part of the eye taken with 200 μm separation between consecutive sections (courtesy Dr. William R Freeman, University of California, San Diego, La Jolla, CA).

through all OCT images (numbering 31 in our case), paying attention to the choroid region, and decides whether the eye is healthy. To this end, the physician needs to first synthesize the choroid region in 3D mentally from 2D OCT sections. This task could be particularly onerous in developing countries, where trained ophthalmologists are few in number. They are often required to examine a large number of such images. Consequently it becomes imperative to develop visualization and quantification tools to help the physician make decisions with less stress.

Various attempts have been made at 3D choroid segmentation and choroid thickness estimation from 2D OCT sections. For instance, a technique involving multiscale Hessian matrix analysis and region growing has recently been reported [2]. Here choroid thickness is estimated by first fitting an upper and a lower envelop on choroid, and then measuring the euclidean distance between those. Another recent technique makes use of 3D edge filtering and projection of probability cones [3]. Graph-based multistage segmentation has also been attempted [4]. The aforementioned works provide proofs of various concepts assuming perfect 3D alignment among OCT sections. However, in practice, perfect alignment is difficult to achieve in view of eye movement, especially, in economical machines suitable for mass deployment in developing countries. Keeping such practical considerations in mind, we shall focus on automated alignment as a first step towards mapping choroid thickness.

Alignment issues in OCT imaging has been reported in various contexts [5]. In the related problem of segmentation of corneal layers, alignment among OCT slices has been attempted using edge detection and quadratic curve fitting [6]. In particular, authors make use of orthogonality of parallel and perpendicular scanned slices. In another work, misalignment due to eye movement has been posed as a tracking problem, and a solution based on particle filtering has been proposed [7]. However, those works do not make use of the innate geometry of the eye, which is approximately spherical. In this paper, we present a systematic analysis of the alignment problem, and cast it as a problem of sphere fitting. Building on geometric alignment, and exploiting the eye structure, we proceed to provide an intensity-based method for isolating the choroid layer, and map its thickness in 3D.

In order to achieve high diagnostic accuracy, one requires not only reliable 3D mapping of choroid thickness, but its appropriate visualization as well. Although the thickness map is generated in 3D, it is generally presented on 2D displays such as a computer monitor. This approach has two main disadvantages. Firstly, in order to comprehend the 3D variation in choroid thickness, one needs to observe the data from various perspectives, i.e., by giving it various rotations. Consequently, for the ophthalmologists, the 3D synthesis still happens mentally, albeit possibly with greater ease than that based on original OCT sections. Secondly, the aforementioned views are generally orthographic projections, and do not correspond to the views one would obtain by looking at a real choroid. Can one overcome these limitations?

Fortunately, the recent lightfield display technology allows life-like 3D reproductions that can be viewed from various angles simultaneously, thus removing both the aforementioned limitations [8]. Indeed 3D visualization of synthetic medical volumetric data using lightfield display has already been demonstrated [9]. In the same vein, we render the isolated choroid on such a display in order to provide the ophthalmologist a stress-free realistic visualization.

The rest of the paper is organized as follows. The proposed geometric methodology is presented in Sec. 2. In Sec. 3, results and pictures illustrating 3D visualization at various steps are presented. Finally, Sec. 4 concludes the paper with a summary of our achievements and the challenges lying ahead.

2. PROPOSED GEOMETRIC APPROACH

We take a geometric approach towards extracting the choroid region, and hence map the spatial variation in choroid thickness. In this section, we shall describe our methodology step by step.

2.1. Methodology

Depicted in Fig. 3, the proposed technique has two major components: spherical alignment of OCT sections, and choroid extraction from aligned sections. Further, spherical alignment is done in three steps. First, certain preprocessing on the OCT slices is performed so as to facilitate the next step of detecting the boundary between the retina and the RPE layers. Finally,

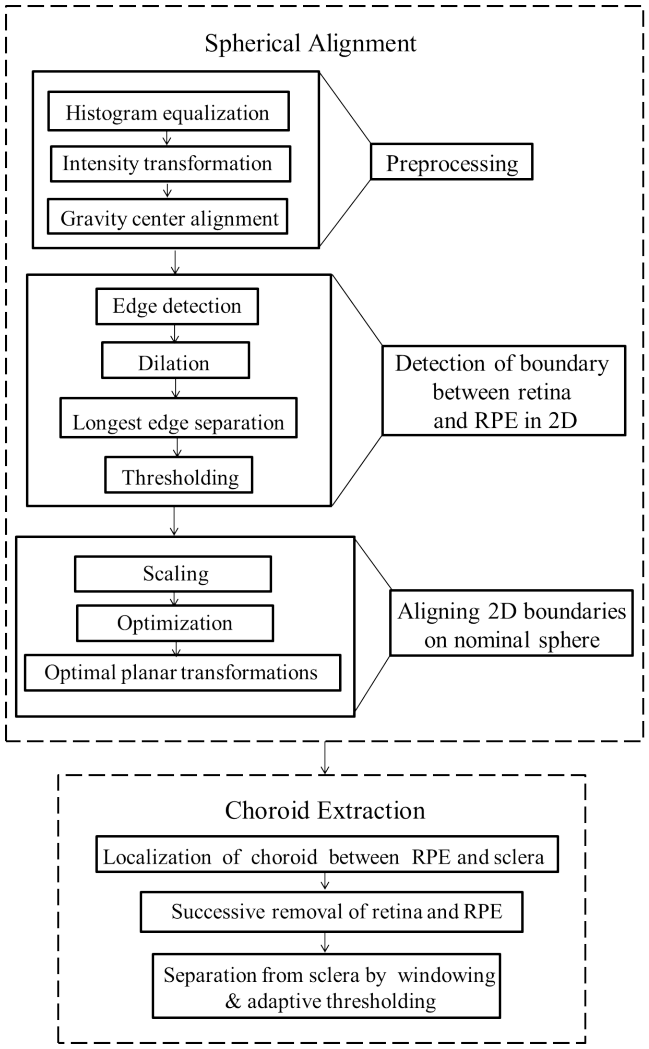

Fig. 3: Proposed methodology as a flowchart

such boundaries from each 2D slice are aligned on the surface of a nominal sphere. Subsequently, the choroid layer is extracted by first localizing it between the RPE and the sclera, then removing the retina and RPE, and finally separating the choroid from sclera by appropriate windowing and adaptive thresholding. Next we provide a detailed description of the proposed method.

2.2. Spherical Alignment

The eye anatomy is nominally a sphere. However, all internal layers of the eye are not spherical (see Fig. 1). For example, the retinal shape deviates considerably from a sphere, especially, near the fovea. Fortunately, the RPE, except in the proximate region of the optic disc, is approximately spherical. In view of this observation, we shall identify the retina-RPE boundary in the OCT sections, and align such boundaries on a nominal sphere. To facilitate boundary detection, we first perform certain preprocessing.

2.2.1. Preprocessing

At this point, let us define the following coordinate axes for the OCT sections. In the en-face image, the horizontal direction corresponds to the Y-axis, while the vertical direction to the Z-axis. Thus OCT slices are parallel to the X-Y plane, where the horizontal direction still corresponds to the Y-axis, while the vertical direction to the X-axis now.

Histogram equalization: As a potential hindrance to the desired boundary detection, the OCT images at hand exhibit varying levels of contrast. For example, in Fig. 2, the 16-th section has higher contrast than the 1-st and 31-st. We first find the best slice in terms of contrast level, and then equalize the histograms of all other slices with respect to the former. This allows us to bring all images to approximately the same level of contrast.

Intensity transformation: Note that the original OCT slices suffer from random offsets relative to each other. Further, subsequent to the desired boundary detection, our goal would be spherical alignment of such boundaries. So, it appears reasonable to attempt to remove such random offsets. In this vein, we propose to align the gravity centers of all slices. However, evaluation of such gravity center could become unreliable in the presence of outliers and background noise. Consequently, we adopt an intensity transformation:

$$I'(x,y) = \begin{cases} 0, & \text{if } I(x,y) < min \\ \frac{255(I(x,y)-min)}{max-min}, & \text{if } I(x,y) \in [min, max] \\ 255, & \text{if } I(x,y) > max, \end{cases}$$

where $I(x,y)$ indicates the image intensity at location (x,y) of the original slice, and $I'(x,y)$ indicates the same after transformation [10]. The threshold values (min, max) are chosen based on the intensity distribution.

Gravity center alignment: As mentioned above, the randomness in the offsets are largely removed via gravity center alignment [10]. To this end, I' obtained in the previous section is used for finding gravity centers (g_x, g_y) as follows:

$$g_x = \frac{\sum_{x=1}^{H}\sum_{y=1}^{W} xI'(x,y)}{\sum_{x=1}^{H}\sum_{y=1}^{W} I'(x,y)} \quad (1)$$

$$g_y = \frac{\sum_{x=1}^{H}\sum_{y=1}^{W} yI'(x,y)}{\sum_{x=1}^{H}\sum_{y=1}^{W} I'(x,y)}, \quad (2)$$

where H denotes the height and W the width of the image. Then gravity centers of all slices are aligned in the XY-plane with respect to some reference gravity center via only translation. In this paper, we make use of OCT sections that are already aligned along Y-axis, and exhibits lack of alignment only in X-coordinates. Accordingly, we shall align the gravity centers only along X-axis.

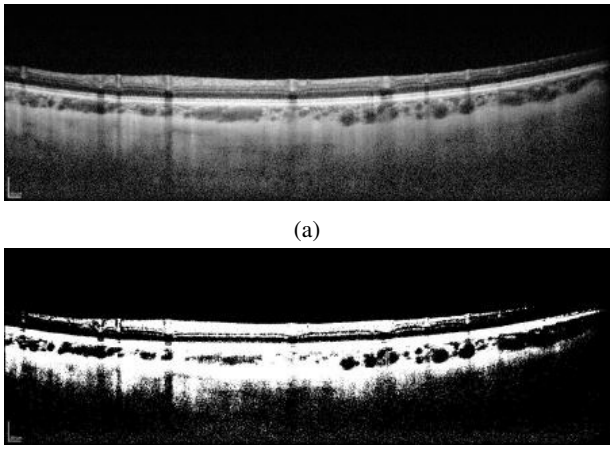

(a)

(b)

Fig. 4: 1-st OCT section: (a) Histogram equalized image; (b) Intensity transformed image.

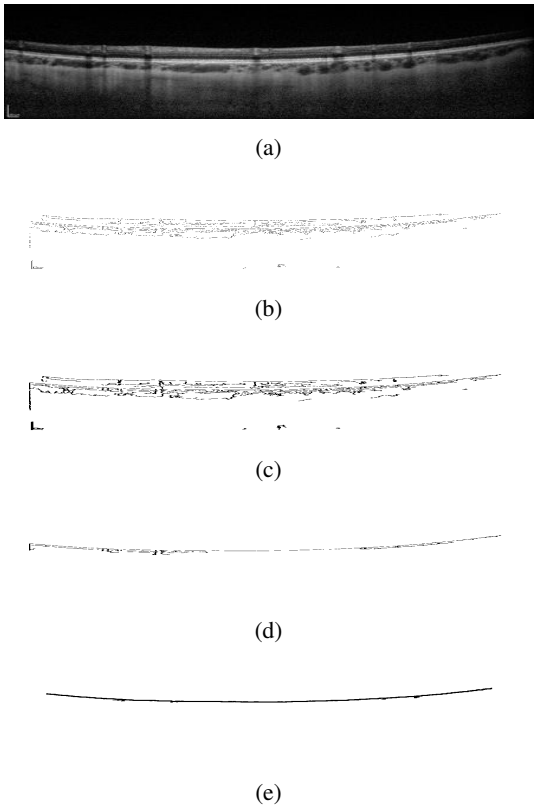

(a)

(b)

(c)

(d)

(e)

Fig. 5: (a) Preprocessed first OCT section; (b) Output of Canny edge detection; (c) Edges after dilation operation; (d) Longest edge extracted by connected components algorithm; and (e) Desired boundary between retina and RPE after thresholding.

2.2.2. Boundary Detection in 2D

Having preprocessed all OCT sections as described above, we are now ready to detect the boundary between the retina and the RPE in each section. To this end, we propose the following steps. We begin by performing edge detection (using, for example, Canny edge operator). Of course, the desired boundary is not expected to feature as a continuous edge. In addition, a large number of edges other than the desired boundary are expected to be detected as well. So, we shall first use dilation to remove discontinuities in the boundary, and then extract the longest edge via connected component algorithm. Finally, the unwanted edges will be removed by appropriate thresholding .

2.2.3. Aligning 2D Boundaries on Nominal Sphere

Next we consider the boundaries found from all the gravity-center-aligned slices, and align them on a nominal sphere. Note that any 3D point (X, Y, Z) lies on the surface of a sphere with center (X_c, Y_c, Z_c) and radius R, if it satisfies

$$(X - X_c)^2 + (Y - Y_c)^2 + (Z - Z_c)^2 = R^2. \qquad (3)$$

Our goal is to find (X_c, Y_c, Z_c) and R that best align the boundaries at hand.

Scaling: Before proceeding further, it is crucial to notice that X-, Y- and Z-axes are sampled at different intervals. So, in preparation to spherical alignment, all axes are scaled (with the help of OCT metadata) so as to endow each axis with the same unit of length.

Optimization: Assuming proper scaling, identify N_i (which should be reasonably large) 3D points $\{(X_{ij}, Y_{ij}, Z_i)\}_{j=1}^{N_i}$ on the retina-RPE boundary on the i-th OCT section, $1 \leq i \leq K$. Here we assume that there are K such sections (in our case, $K = 31$). Our task is to provide a planar transformation (which possibly varies from slice to slice) to each OCT slice in such a manner that the transformed points deviate the least from a nominal sphere. Since Y-coordinates are already aligned, we shall consider planar transformations that alters the X-coordinate, but leaves the Y- and Z-coordinates unchanged. Finally, we shall leave the first and the last sections unaltered in order to avoid ambiguity.

Formally, such planar transformation for the i-th ($1 \leq i \leq K$) section takes the form $T_i : (X_{ij}, Y_{ij}, Z_i) \to (X'_{ij}, Y'_{ij}, Z'_i)$, where

$$X'_{ij} = \alpha_i X_{ij} + \beta_i Y_{ij} + \gamma_i$$

for some $(\alpha_i, \beta_i, \gamma_i)$, $Y'_{ij} = Y_{ij}$ and $Z'_i = Z_i$. Further, we fix

$$(\alpha_i, \beta_i, \gamma_i) = (1, 0, 0) = (\alpha_K, \beta_K, \gamma_K),$$

i.e., $X'_{ij} = X_{ij}$ for each $1 \leq j \leq N_i$ as long as $i = 1$ or $i = K$.

Thus our task boils down to solving the following opti-

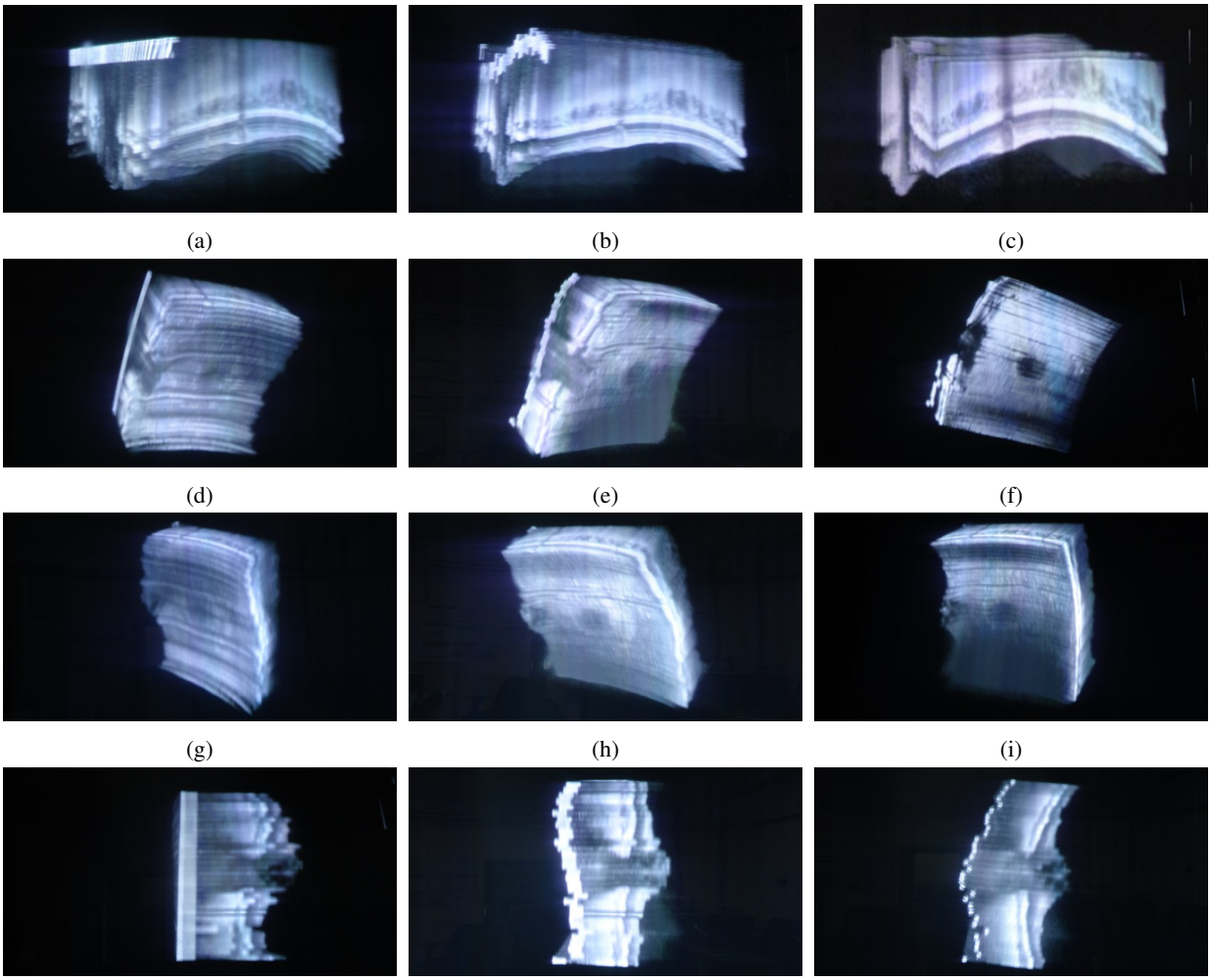

Fig. 6: 3D visualization using lightfield display: (a), (d), (g), and (j) – various perspectives of unaligned OCT sections; (b), (e), (h), and (k) – corresponding perspectives after performing gravity center alignment; (c), (f), (i), and (l) – corresponding perspectives after performing spherical alignment.

mization problem:

$$(\Phi^*, \Psi^*) \quad = \quad \arg\min_{(\Phi,\Psi)} \sum_{i=1}^{K} \sum_{j=1}^{N_i} ((X'_{ij} - X_c)^2 + (Y_{ij} - Y_c)^2 + (Z_i - Z_c)^2 - R^2)^2. \quad (4)$$

where we optimize the center (X_c, Y_c, Z_c) and radius R of the nominal sphere, denoting $\Phi = \{X_c, Y_c, Z_c, R\}$ for convenience, jointly with the free planar transformation parameters $\Psi = (\alpha_i, \beta_i, \gamma_i)_{i=2}^{K-1}$.

Optimal planar transformations: The optimal choice of Ψ^* in (4) specifies the collection of optimal planar transformations T_i, $2 \leq i \leq K-1$. So, in order to achieve spherical alignment, it is tempting to simply transform the i-th preprocessed section, $2 \leq i \leq K-1$. However, this method generally maps a point on the integer grid to a point that does not lie on the integer grid on the transformed axes. Appropriate interpolation will be performed to obtain image values on the desired integer grid.

2.3. Choroid Extraction

Having achieved spherical alignment using retina-RPE boundary, and localized choroid between RPE and sclera, we begin by noticing that the inner side of the boundary consists of retina only, and hence removing it. The RPE layer has more or less uniform thickness, and its outer boundary with choroid can be detected with edge and related operations as mentioned earlier. Using this, next we remove the RPE, and are only left to remove the sclera. We complete this task in several steps. First a concentric outer sphere is introduced, and the mass lying outside is discarded. This removes a large part of the

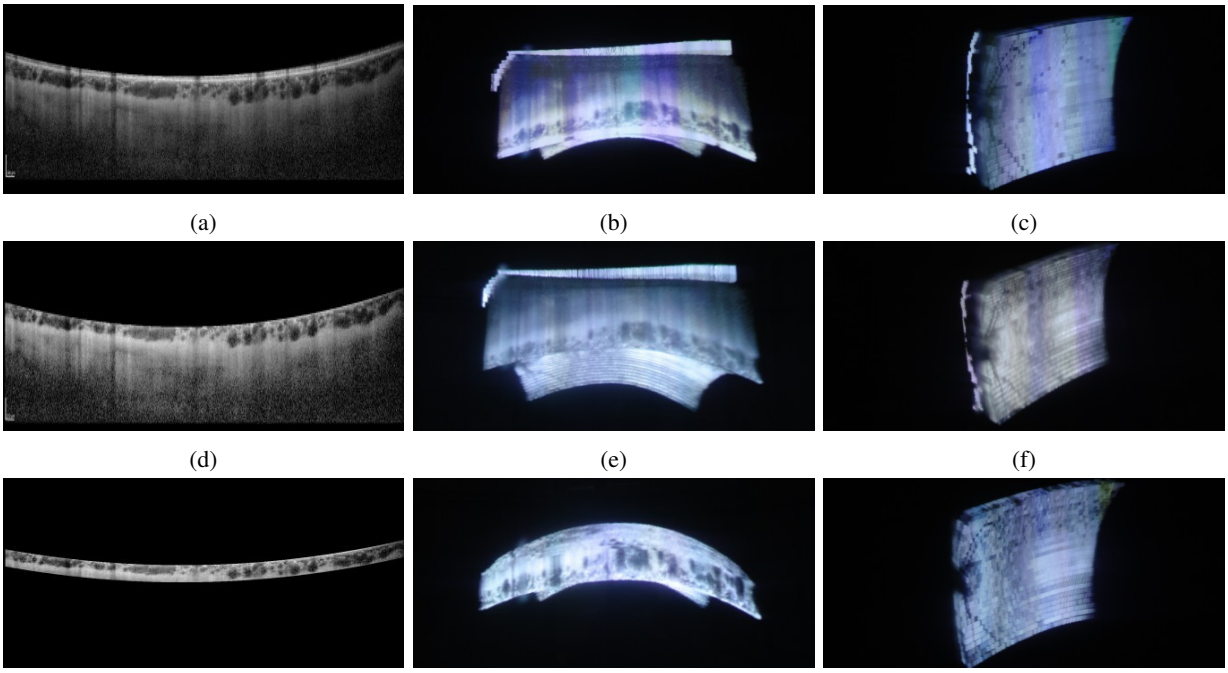

Fig. 7: Step-by-step extraction of choroid: (a), (b), (c) Removing retina; (d), (e), (f) Removing RPE; (g), (h), (i) Crude removal of sclera; (a), (d), (g) correspond to first OCT section (2D); (b), (e), (h), and (c), (f), (i) correspond to two perspectives in 3D visualization, respectively.

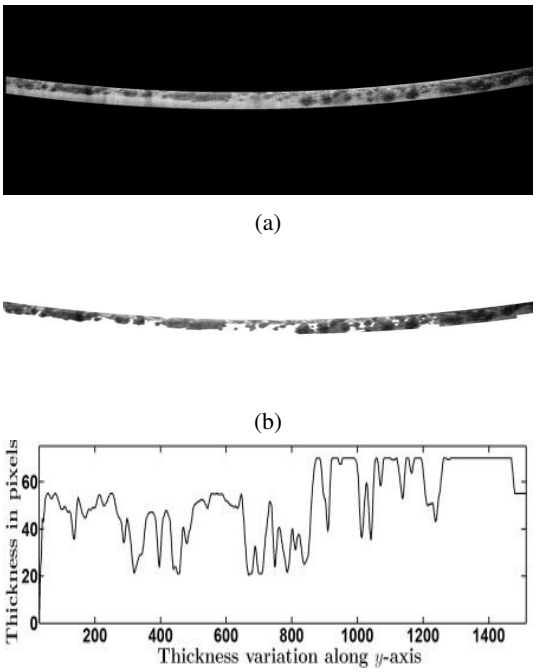

Fig. 8: First OCT section — processing in 2D: (a) Crude extraction of choroid; (b) Refinement of extracted choroid; (c) Quantification of choroid thickness.

sclera. We further refine the extracted choroid by windowing and adaptive thresholding. Finally, we visualize the extracted choroid, and map its thickness.

3. RESULTS

In this section, we illustrate our methodology using the aforementioned OCT sections (see Fig. 2), and present our results.

3.1. Spherical Alignment

Among our OCT images, the 11-th section was found to have the highest contrast. Accordingly, all images are histogram equalized with respect that section. Further, their intensities are transformed. See Fig. 4 for the histogram equalized and intensity transformed first slice. Preprocessing is completed by aligning their gravity centers. The boundary between the retina and the RPE is detected in each preprocessed slice. Specifically, edge detection using Canny operator, dilation, longest edge separation, and appropriate thresholding are performed. The results are shown for the first slice (Fig. 5a). Edge detection results in many spurious edges along with the desired edge (Fig. 5b), which suffers from discontinuities. Such edge discontinuities are removed by dilation (Fig. 5c). Noting that the edge between the retina and the RPE constitutes the longest edge, connected component algorithm is ap-

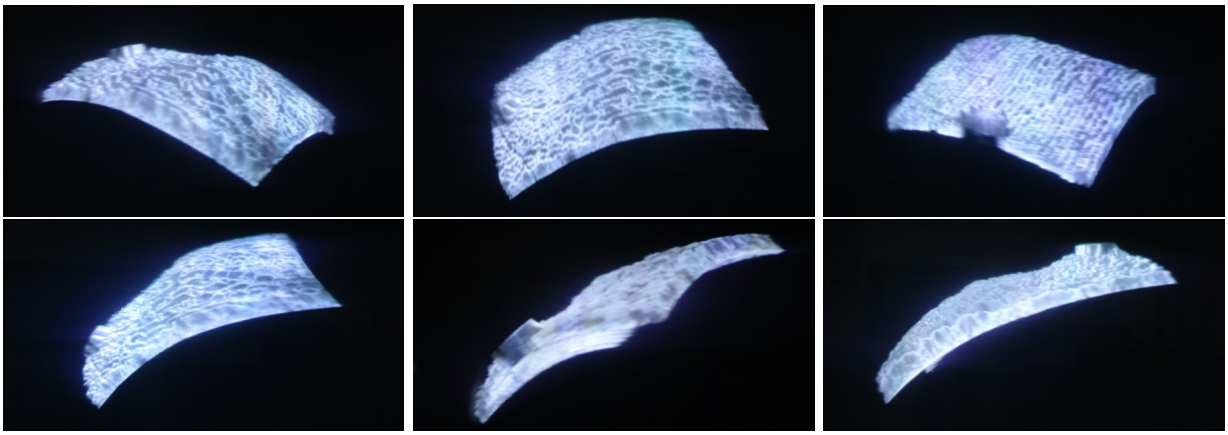

Fig. 9: 3D visualization: various views of extracted choroid layer.

plied to extract that (Fig. 5d). Surviving unwanted edges and points are then removed by appropriate thresholding (Fig. 5e).

Next we successively perform gravity center alignment and spherical alignment, and visualize in 3D the corresponding effect with reference to stacked unaligned sections. In our experiment, we made use of a lightfield display (Holovizio 721RC). However, here we include several 2D views for easy appreciation by the reader. In Fig. 6, the leftmost column presents the reference unaligned sections, the middle column the gravity center aligned sections, and the rightmost column the spherically aligned sections. In each row, approximately same perspective is maintained for easy comparison. Notice that the spherically aligned sections stack up to approximate the natural geometry. Indeed those highlight a circular fovea indicating proper alignment.

3.2. Choroid Visualization and Thickness Mapping

Having detected and spherically aligned the retina-RPE boundary, we proceed to peel of the retina and the RPE in succession. Then we crudely extract the choroid by removing the major portion of sclera using a concentric sphere as a spatial threshold. In Fig. 7, the aforementioned steps are demonstrated. Specifically, these steps are illustrated in 2D in the leftmost column using our first OCT section. The same steps are again presented in 3D in the middle and the rightmost columns from two different perspectives.

Next the crudely extracted choroid is refined by separating the remaining part of sclera with the help of windowing and adaptive thresholding. Finally, the choroid thickness is quantified via appropriate smoothening to avoid discontinuous estimates. These steps are illustrated in 2D in Fig. 8 using our first OCT section.

Further, the choroid layer is visualized in 3D from six different perspectives in Fig. 9. Notice the depletion in choroid thickness in the vicinity of the optic disc. In this connection, recall that the presented images are pictures taken of the 3D rendering on a lightfield display. In practice, the depletion stands out more dramatically. In view of this, we believe the proposed 3D visualization will come to the aid of ophthalmologists.

To complement 3D visualization of the extracted choroid, we also quantify and spatially map its thickness. The basic principle remains the same as demonstrated in Fig. 8; only the presentation and some smoothening are now performed in 3D. The mapped choroid thickness is first visualized on the lightfield display (Fig. 10a), and then using MATLAB on a regular computer terminal (Fig. 10b). Not surprisingly, the former provides a more realistic feel of the natural geometry. We also present the thickness distribution from the *en-face* perspective (Fig. 10c). Of course, the last plot is in 2D, and is better visualized on 2D monitors (due to superior 2D resolution compared to the lightfield display). Hearteningly, all the various modes of proposed representations indicate appreciable depletion in choroid thickness in the vicinity of the optic disc.

4. DISCUSSION

In summary, we propose a 3D visualization and mapping approach to diagnosis based on choroid thickness. The main challenge arises from the fact that choroid represents an inner layer of posterior part of the eye. Our main contribution lies in exploiting the nominally spherical geometry of the eye, and aligning the OCT sections to their natural setting. We further propose the lightfield display as a diagnostic tool, on which the spatial variation of choroid thickness can be visualized in its natural geometric context. The effectiveness of the proposed methodology is demonstrated using real-life OCT images.

In this paper, we put forward a proof of concept, which needs further improvement. To begin with, the eye geometry is nominally spherical, but not exactly so. In future, we plan to incorporate the flexibility of small deviation from the

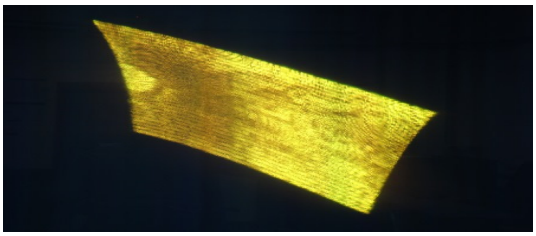

(a)

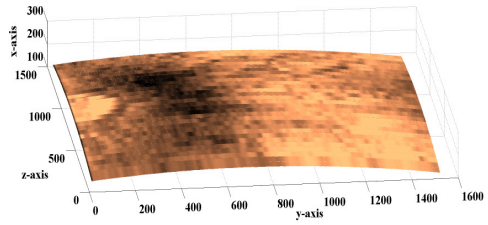

(b)

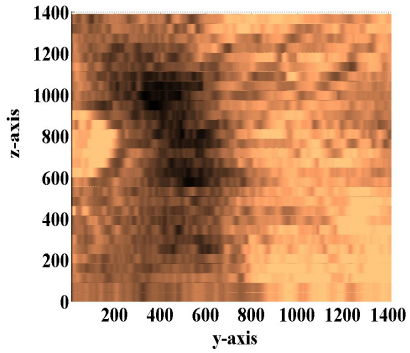

(c)

Fig. 10: Visualization of spatial distribution of choroid thickness: (a) On 3D light filed display; (b) 3D plot in Matlab; (c) *en-face* plot in Matlab.

spherical geometry via local processing. Further, the current inter-section resolution of 200 μm is not fine enough, and leads to visual jumps in our Z-axis. To avoid it, we plan to incorporate suitable interpolation. In addition, statistical methods of choroid vessel segmentation and tracing would add considerable value to our proposed technique.

5. REFERENCES

[1] `http://webvision.med.utah.edu`

[2] L. Zhang, K. Lee, M. Niemeijer, R. F. Mullins, M. Sonka, and M. D. Abràmoff, "Automated segmentation of the choroid from clinical SD-OCT," *Investigative ophthalmology & visual science*, vol. 53, no. 12, 7pp. 510–7519, 2012.

[3] V. Kajić , E. Marieh, G. Carl, F. K. Martin, H. Joachim, O. Richu, B. Susanne, G. F. James, and D. Wolfgang, "Automated three-dimensional choroidal vessel segmentation of 3D 1060 nm OCT retinal data," *Biomedical optics express*, vol. 4, no. 1, pp.134, 2013.

[4] Z. Hu, X. Wu, Y. Ouyang, Y. Ouyang, and S. R. Sadda, "semiautomated segmentation of the choroid in spectral-domain optical coherence tomography volume scans," *Investigative ophthalmology & visual science*, vol. 54, no. 3,pp. 1722–1729, 2013.

[5] I. Marín-Franch, W. H. Swanson, B. R. Adams, H. Zhu, and D. P. Crabb, "Novel Analytical Methods for Stratus OCT: Alignment of the Scan Circle," *Optometry and Vision Science* vol. 89, no. 12, pp. e109–e111, 2012.

[6] J. A. Eichel, K. K. Bizheva, D. A. Clausi, and P. W. Fieguth, "Automated 3D Reconstruction and Segmentation from Optical Coherence Tomography," 11^{th} *European conference on computer vision conference on Computer vision (ECCV'10), Part III, Springer,* LNCS, vol. 6313, pp. 44–57, 2010.

[7] J. Xu, H. Ishikawa, G. Wollstein, L. Kagemann, and J. S. Schuman, "Alignment of 3-D optical coherence tomography scans to correct eye movement using a particle filtering," *IEEE Transactions on Medical Imaging*, vol. 31, no. 7 pp. 1337–1345, 2012.

[8] T. Balogh, P. T. Kovács, Z. Dobrányi, A. Barsi, Z. Megyesi, Z. Gaál, and G. Balogh, "The Holovizio systemNew opportunity offered by 3D displays," *In proceedings of the International Symposium on Tools and Methods of Competitive Engineering (TMCE)*, pp. 79–89, 2008.

[9] M. Agus, F. Bettio, A. Giachetti, E. Gobbetti, J. A. I Guitian, F. Marton, J, Nilsson, G. Pintore, "An interactive 3D medical visualization system based on a light field display," *The Visual Computer Journal, Springer*, Vol. 25, Issue 9, pp. 883–893, September 2009.

[10] V-F. Zaharescu, "Semi-automatic Volume Slices Alignment for 3D Reconstruction and Analysis," *Diploma Thesis*, University of Bucharest, June 2001.